

## Biomorphic Charcoal/TiO<sub>2</sub> Composites from Poplar Templates

Liangcun Qian,<sup>a,b</sup> Peirong Chen,<sup>b</sup> Rui Li,<sup>a,b</sup> Lin Mei,<sup>a,b</sup> Yamei Liu,<sup>a</sup> Geli Wu,<sup>a</sup> and Shengquan Liu<sup>a,\*</sup>

Biomorphic charcoal/TiO<sub>2</sub> composites (C/TiO<sub>2</sub>) were produced from poplar templates. The poplar templates were impregnated with butyl titanate sol with a vacuum/positive pressure technology. From the anatomic structure of poplar and fluid thermodynamics, the alternative vacuum/positive pressure technology was an efficient method of infiltrating bio-templates with sol and overcoming the embolization effect of the sol in capillaries. After sol infiltration, the maximum density of the poplar was approximately  $0.958 \pm 0.005$  g/cm<sup>3</sup>. Using X-ray diffraction (XRD), thermogravimetric data (TG-DTG), and scanning electron microscopy (SEM), it was found that the pore sizes in the cell walls of C/TiO<sub>2</sub> were, respectively, 30 to 150, 3 to 15, and 1.5  $\mu$ m, and a surprising mesoporous-like honeycomb structure formed at approximately 800 °C in a N<sub>2</sub> atmosphere. The phase structure of C/TiO<sub>2</sub> shifted from anatase to rutile between 700 and 900 °C in N<sub>2</sub>. Furthermore, the temperature of the maximum combustion rates of C/TiO<sub>2</sub> sintered at 800 °C in N<sub>2</sub> was approximately 610 °C. The average shrinkage values from the native poplar to C/TiO<sub>2</sub> along the radial, tangential, and axial directions were 28.53%, 21.80%, and 17.03%, respectively.

*Keywords:* Mesoporous; Biomorphic C/TiO<sub>2</sub> composites; Anisotropic; Vacuum technology

*Contact information:* a: College of Forestry and Gardening; b: School of Science, Anhui Agricultural University, Hefei, 230036, P.R. China; \*Correspondence author: Liusq@ahau.edu.cn

### INTRODUCTION

As forest resources change in China, fast-growing poplar wood has become an important commercial resource (Wu *et al.* 1998). However, the surface of dried poplar is prone to twisting and shrinking because of the flaws in the grain and an unstable dimension. The flaws in the grain cause practical problems for decorating board and structural wood (Shahverdi *et al.* 2012). Hence, wood researchers are very interested in the potential applications of poplar wood as the biomass materials and the biotemplates. Its anatomic structure makes it accessible to gaseous or aqueous infiltration and suitable for producing porous biomorphic composites (Colombo 2006). Using natural wood and its charcoal as templates for producing inorganic materials is an effective strategy to obtain controllable materials with biomorphic porous microstructure (Li *et al.* 2012; Qian *et al.* 2015).

Titania (TiO<sub>2</sub>) is a promising semiconductor material that is extensively used in photocatalytic experiments because of its chemical stability, long broadband, and super-hydrophilic performance (Chen and Mao 2007). Different types of porous ceramics, *e.g.* TiO<sub>2</sub> and TiN/Charcoal (TiN/C), have been fabricated using various methods (Luo *et al.*

2007; Qian *et al.* 2015); however, biomorphic charcoal/titania (C/TiO<sub>2</sub>) composites from poplar templates are relatively unexplored.

In this paper, the infiltration behavior of butyl titanate sol was investigated on poplar wood, and vacuum/positive pressure technology was used to initiate sol-gel infiltration into hardwood. Furthermore, C/TiO<sub>2</sub> composites were produced from poplar templates. The biomorphic structures, crystalline phase, and pyrolysis behavior of the C/TiO<sub>2</sub> composites were characterized by scanning electron microscopy (SEM), thermogravimetric analysis (TGA), and X-ray diffraction (XRD), respectively. Additional physical characteristics elucidated the mechanism of the C/TiO<sub>2</sub> composite formation.

## EXPERIMENTAL

### Materials and Reagents

Chemical grade butyl titanate Ti(OC<sub>4</sub>H<sub>9</sub>)<sub>4</sub> and analytical grade acetic acid (CH<sub>3</sub>COOH), anhydrous ethanol (CH<sub>3</sub>CH<sub>2</sub>OH), and benzene (C<sub>6</sub>H<sub>6</sub>) were purchased from the Sinopharm Chemical Reagent Co. Ltd., Shanghai, China. All reagents were used without further purification. The purity of nitrogen (N<sub>2</sub>) was 99.999%.

Specimens of poplar (*Populus × euramericana*) were harvested from the Forest Farm at Anhui Agricultural University, Anhui Province, China. Native poplars of up to 12 years of age were cut into chips of three sizes (Table 1). All samples were dried at 103 °C for 10 h and pretreated in a Soxhlet apparatus with benzyl alcohol (1:2 volume ratio of benzene to 95% ethanol) at 90 °C for 24 h under reflux to remove extracts containing tannins and fatty acids. Finally, all samples were dried at 90 °C for 24 h.

**Table 1.** Dimensions of Native Poplar and C/TiO<sub>2</sub> Composites

Wood Type	Group	Average Dimensions*			Volume (cm <sup>3</sup> )
		Radial (mm)	Tangential (mm)	Longitudinal (mm)	
Native Poplar	1	19.46 ± 0.03	19.83 ± 0.03	7.55 ± 0.01	5.139 ± 0.005
	2	19.66 ± 0.03	19.64 ± 0.03	12.09 ± 0.02	
	3	19.49 ± 0.03	19.90 ± 0.03	20.20 ± 0.03	
C/TiO <sub>2</sub> Composite	1	15.22 ± 0.02	13.76 ± 0.02	6.35 ± 0.01	2.397 ± 0.003
	2	15.11 ± 0.02	14.26 ± 0.02	9.95 ± 0.01	
	3	15.50 ± 0.02	14.40 ± 0.02	16.66 ± 0.02	

\*Means ± standard deviation

### Composite Preparation

Ti(OC<sub>4</sub>H<sub>9</sub>)<sub>4</sub>, CH<sub>3</sub>COOH, and CH<sub>3</sub>CH<sub>2</sub>OH (volume ratio of 68:12:50) were stirred for 2 h at room temperature to obtain the TiO<sub>2</sub> sol. The extracted samples were immersed in TiO<sub>2</sub> sol for 7 days and subsequently subjected to infiltration in an adjustable air pressure dipping can at a vacuum pressure of 1.00 kPa for 30 min and positive air pressure of 2.00 MPa for 30 min. Finally, all samples were removed from the sol. The sol absorbed water from air for 12 h, resulting in the formation of Ti(OC<sub>4</sub>H<sub>9</sub>)<sub>4</sub> gelatin, CH<sub>3</sub>COOH, and CH<sub>3</sub>CH<sub>2</sub>OH. All samples were dried at 130 °C for 2 h to obtain the TiO<sub>2</sub>

gel *in situ*. The infiltration-drying process was repeated three times to increase the gel content of the samples. To produce C/TiO<sub>2</sub>, all samples were pyrolysed at 800 °C for 1 h in N<sub>2</sub>.

### Characterization

The phase structure of TiO<sub>2</sub> after sintering was identified by an XD-3 X-ray diffractometer (PERSEE, Beijing, China), operating with Cu K $\alpha$  radiation ( $\lambda = 1.540563$  Å), a scan rate of 1°/min, accelerating voltage of 36 KV, applied current of 20 mA, and diffraction angle ( $2\theta$ ) ranging from 10° to 70°. The anatomic structures of the biomorphic charcoals and C/TiO<sub>2</sub> composites from the poplar templates were observed with a Hitachi S-4800 scanning electron microscope (Tokyo, Japan). Therefore, the different families and distribution of porous sizes were visualized from the formed pores.

A thermogravimetric (TG) analyzer (TG-209, NETZSCH, Selb, Germany) was used to analyze the thermal stability of the C/TiO<sub>2</sub> composites; it was operated with purged air at a flow rate of 20 mL/min. The C/TiO<sub>2</sub> powder (10.0 mg) was loaded into the alumina crucible on the TG-209 and heated at 10 °C/min from 40 to 700 °C. The corresponding mass remnants (TiO<sub>2</sub>) and thermal stability of C/TiO<sub>2</sub> composites were analyzed through the TG-DTG profiles. The slope of the TG profile indicated the speed of mass loss (MS). Therefore, the average speed of MS (*slope*) was calculated using Eq. 1, where  $\Delta t$  is the variation in temperature during the loss of the sample mass ( $\Delta M$ ):

$$\text{slope} = \frac{\Delta M\%}{\Delta t} \quad (1)$$

The DTG profiles were also expressed as the rate of MS. The value of  $T$  was defined as each temperature at which the differential of DTG profiles equal to zero, *i.e.* the inflection point for temperature in the DTG profiles. Therefore, the  $T_1$ ,  $T_2$ , and  $T_3$  were expressed, respectively, as the ignition temperature at the first inflection point of the DTG profiles, the burnout temperature at the last inflection point of the DTG profiles, and the temperature of the maximum combustion rate in the bottom inflection point of the DTG profiles according of Eq. 2 and the burnt process (Sun *et al.* 2010):

$$\frac{d^3 M\%}{dt^3} = 0 \quad (2)$$

The mass of the samples ( $M$ ) was measured using a balance with a precision of 0.001 g, and sample volumes ( $V$ ) were measured using vernier calipers with a precision of 0.01 mm. Densities ( $\rho$ ) were calculated using Eq. 3:

$$\rho = \frac{M}{V} \quad (3)$$

The dimensions of the samples consistently shrank during the annealing process. Therefore, the dimensions of the native samples ( $L_0$ ) and annealing samples ( $L$ ) were measured, and the shrinkage rates ( $SR$ ) were calculated using Eq. 4:

$$SR(\%) = \frac{L_0 - L}{L_0} \times 100 \quad (4)$$

## RESULTS AND DISCUSSION

### Extraction in Benzyl Alcohol

After extracting poplar, the benzyl alcohol solution was a pale yellow color, indicating that inclusion materials (tannin, fat, *etc.*) had been removed from the cell cavities. These spaces could thus be impregnated with the  $\text{Ti}(\text{OC}_4\text{H}_9)_4$  sol-gel.

### Sol-gel Processing

The complete distribution of sol-gel in the cells depends on the structure of the individual cell cavities. Bordered pits in the secondary wall of the hardwood cell leave a visibly open passageway between cells (Fig. 1). The typical bordered pit in poplar contains a membrane (1), chamber (2), aperture (3), margo (4), and torus (5) (Zwieniecki and Holbrook 2000). The membranes supporting the margo are flexible and allow the rigid torus to be displaced laterally by surface tension against one of the apertures, which forms an aspirating pit. Thus, the pit closes or partly closes to resist the passage of liquids; this phenomenon explains the lack of permeability in poplar cells. Pit aspirations prevent air bubbles from entering the translocation stream as the result of injury during forest growth. However, during sol infiltration, the embolism of pits (Fig. 1c) prevents air bubbles from escaping the translocation stream (Choat *et al.* 2008). Consequently, the vacuum and alternative positive pressure promoted the movement of the pit torus so that the sol perfused into the cell cavities.

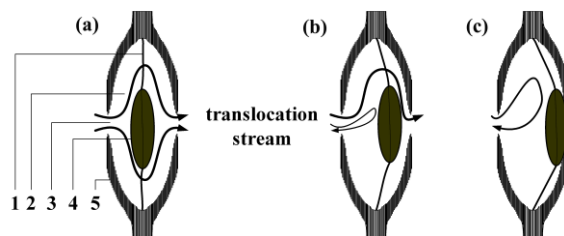


**Fig. 1.** Pit structures in hardwood: (a) aspirating pit, (b) partly closed pit, and (c) closed pit. (1) Membrane, (2) chamber, (3) aperture, (4) margo, and (5) torus

The transport of the sol in the fusiform fibres must overcome the embolization effect in capillaries. Many fusiform fibres are arranged in an orderly manner within the dried hardwood (Fig. 2(a); Choat *et al.* 2008). When the sol infiltrates hardwood, air bubbles in the fibre form embolisms in cell cavities. There are many apertures at the two ends of a fusiform fibre and in the cell walls, and these apertures allow the exchange of water and nutrients. As the sol passes through fibres, there are always air bubbles in the flowing sol stream. Because the fluid thermodynamics of surface tension around an air bubble results in spherical shapes (Fig. 2(b)), the pressure on the concave surface of bubbles is always pointed toward the centre of the sphere, and the classical Laplace-Young's equation is applicable (Eq. 5),

$$P = \frac{2\alpha}{R} \quad (5)$$

where  $P$ ,  $\alpha$ , and  $R$  are the pressure from surface tension, the liquid coefficient of surface tension around the air bubble, and the radius of the air bubble, respectively.  $P$  is inversely proportional to  $R$ , and  $R$  decreases along the direction of the sol stream when sol enters

the fusiform fibre. Conversely,  $R$  increases against the direction of the sol stream (Fig. 2(c)). As a result,  $P_2$  and  $P_4$  decrease, but  $P_1$  and  $P_3$  increase. The total pressure ( $P_0$ ) equals  $P_1 + P_3 - P_2 - P_4$ . The direction of  $P_0$  on the concave surface of bubbles is always in the opposite direction of the sol stream. Consequently, it hinders sol flow in fusiform fibres. Embolization occurs in fusiform fibres when  $P_0$  is strong.

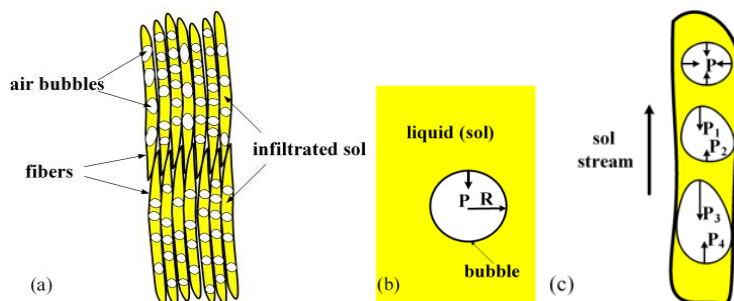


**Fig. 2.** The dynamics of sol infiltration of fusiform fibers: (a) sol infiltrating fusiform fibers, (b) air bubble suspended in liquid, and (c) sol flowing in fusiform fibers

However, negative pressure around the fibres removes most air bubbles from the infiltrated sol and the fusiform cellular templates; positive pressure reduces the volume and radius of the air bubbles. The combined effect of the vacuum/positive pressure destroys embolisms in impregnated fibres. Thus, poplar templates were treated with this method to allow complete and homogenous impregnation of the fibres.

**Table 2.** Geometrical Densities of Poplar Templates after Sol-Gel Infiltration

Number of Infiltrations	Geometrical Densities (g/cm <sup>3</sup> )		
	Group 1	Group 2	Group 3
0	0.348 ± 0.003	0.365 ± 0.003	0.372 ± 0.003
1	0.911 ± 0.005	0.875 ± 0.004	0.805 ± 0.004
2	0.955 ± 0.005	0.911 ± 0.005	0.880 ± 0.004
3	0.958 ± 0.005	0.909 ± 0.005	0.860 ± 0.004
Average	0.909 ± 0.005		

The poplar templates were dried at 130 °C for 2 h to evaporate ethanol and acetic acid from the samples. The sol-gel process was repeated three times; Table 2 shows the geometrical densities of the poplar samples. The sample densities increased after the first and second impregnation, but there was very little change in sample density between the second and third impregnation. Thus, two cycles of impregnation were sufficient to fill most cell cavities. The weight of impregnated samples was more than two times that of the native dried poplar. After sol infiltration, the maximum density of the poplar was close to 0.958 ± 0.005 g/cm<sup>3</sup>.

### TiO<sub>2</sub> Phase Structure

The phase structure of TiO<sub>2</sub> was monitored by XD-3 in the C/TiO<sub>2</sub> composites from 400 °C to 900 °C (Fig. 3). The diffraction peaks at 25.2°, 37.8°, 48.1°, and 55.2°

were assigned to the diffractions of the (101), (004), (200), and (211) planes of anatase TiO<sub>2</sub> (JCPDS number 21-1272) (Yang *et al.* 2009). The diffraction peaks at 27.5°, 36.0°, 41.5°, and 54.0° were assigned to the diffractions of the (110), (101), (200), and (211) planes of rutile TiO<sub>2</sub> (JCPDS number 21-1276) (Chen and Mao 2007). The anatase structure was observed at 400 °C. The phase structure shifted from anatase to rutile between 700 °C and 900 °C; the TiO<sub>2</sub> structure was completely rutile at 900 °C. The TiO<sub>2</sub> phase transition temperature from anatase to rutile was notably increased in a nitrogen atmosphere compared with an air atmosphere, owing to an inert atmosphere and the presence of reducing charcoals. When the temperature increased, the intensity of TiO<sub>2</sub> diffraction peaks also increased. Thus, the temperature and nitrogen atmosphere greatly influenced the crystal structure and crystallization level.

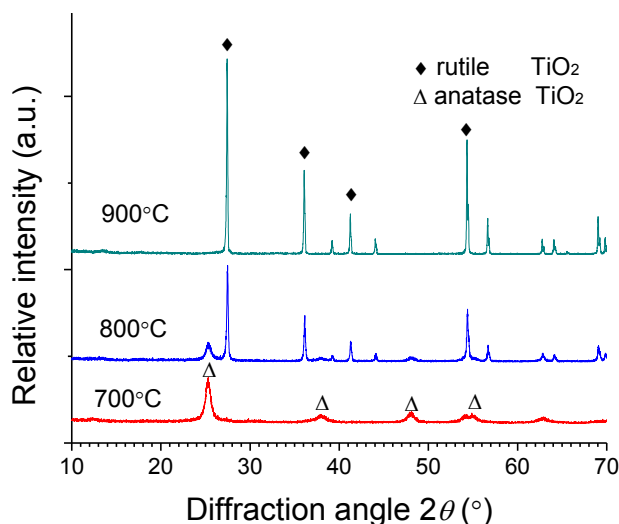


**Fig. 3.** The XRD patterns of the C/TiO<sub>2</sub> composites

### TG-DTG Analysis

The C/TiO<sub>2</sub> composites were sintered at 400 °C (400C/TiO<sub>2</sub>) and 800 °C (800C/TiO<sub>2</sub>) in N<sub>2</sub>. The profile curves of their oxygenolysis below 700 °C are shown in Fig. 4(a). Comparing the TG curves of 400C/TiO<sub>2</sub> with the TG curves of 800C/TiO<sub>2</sub>, the results showed that the 400C/TiO<sub>2</sub> composites below 290 °C and the 800C/TiO<sub>2</sub> composites below 350 °C were stable in an air atmosphere (Qian *et al.* 2015; Sun *et al.* 2010). Furthermore, the ignition temperature of the 400C/TiO<sub>2</sub> composites in air was obviously lower than that of the 800C/TiO<sub>2</sub> composites. The corresponding remnants (TiO<sub>2</sub>) were estimated to be approximately 76.11% and 77.46%, respectively, and the corresponding temperatures for removal of the charcoal templates were approximately 520 and 640 °C, respectively. From the slopes of the TG profiles, the averages calculated using Eq. 3 were 0.1550%/°C (slope 1) and 0.0798%/°C (slope 2), respectively. These results suggest that the C/TiO<sub>2</sub> composites sintered at higher temperatures in N<sub>2</sub> resulted in more sufficient pyrolyzing and were more stable in air (Gu *et al.* 2007).

The ignition temperature ( $T_1$ ), the burnout temperature ( $T_2$ ), and the temperature of the maximum combustion rate ( $T_3$ ) were calculated using Eq. 2, respectively. The DTG curves revealed that the burnout temperatures of 400C/TiO<sub>2</sub> and 800C/TiO<sub>2</sub> were at approximately 536 °C and 658 °C, respectively (Fig. 4b). Furthermore, the temperature of the maximum combustion rate of the 400C/TiO<sub>2</sub> in air was approximately 430 °C;

however, the temperatures of the maximum combustion rate of the 800C/TiO<sub>2</sub> sample were at approximately 510 °C and 610 °C, respectively. It appeared that the tight packing of TiO<sub>2</sub> around the charcoal on the surface of the 800C/TiO<sub>2</sub> composites hindered oxygenolysis below 510 °C, resulting in a flame retardant effect (Mahr *et al.* 2012). Conversely, gaps between the charcoal and the TiO<sub>2</sub> in the 800C/TiO<sub>2</sub> composites allowed their rapid oxygenolysis between 610 °C and 660 °C (Deka and Maji 2011). The results indicated that the temperature of the sintered C/TiO<sub>2</sub> composites in N<sub>2</sub> had a remarkable effect on the removal of charcoal templates. In addition, the 800C/TiO<sub>2</sub> was more difficult to remove from the charcoal templates than the 400C/TiO<sub>2</sub>. This result showed that the C/TiO<sub>2</sub> composites sintered at a higher temperature in N<sub>2</sub> were more stable in air.

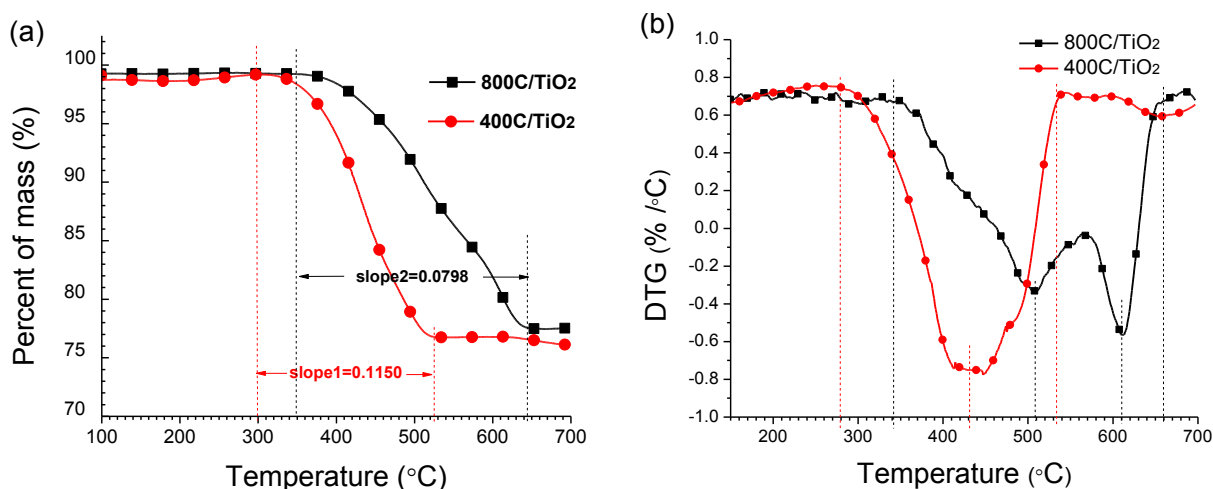
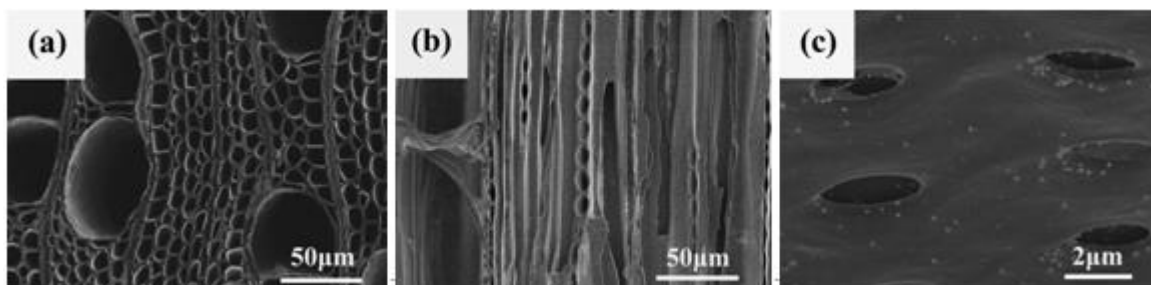


**Fig. 4.** The thermal stability curves of C/TiO<sub>2</sub> sintered at 400 °C and 800 °C, respectively: (a) TG curves, and (b) DTG curves

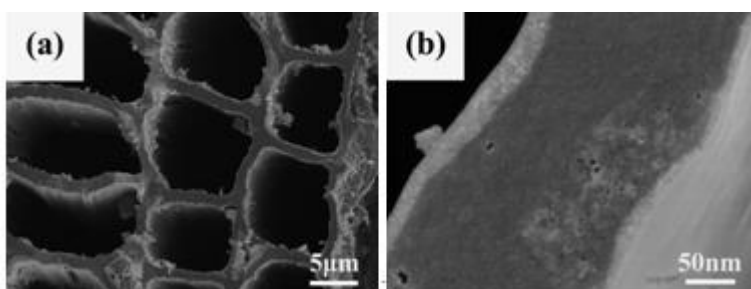
### Microstructure Analysis

Figure 5 shows SEM images of the poplar charcoals sintered at 800 °C in N<sub>2</sub>. Three pore sizes were analyzed: 30 to 150 μm, 3 to 15 μm, and approximately 1.5 μm (Kurosaki *et al.* 2003). The first pores originated from the vessels in Fig. 5(a); the second originated from fusiform fibres and ray cells (Fig. 5(b)). The third pores originated from pitting groups (Fig. 5(c)). The fibres sintered at 800 °C in N<sub>2</sub> exhibited pit membranes that were cracked and weakened to form the pit pores.

Figure 6 shows SEM images of the C/TiO<sub>2</sub> composites from the poplar templates sintered at 800 °C in N<sub>2</sub>. Not only did the C/TiO<sub>2</sub> composites with TiO<sub>2</sub> crystal grains adhering to the charcoal walls exactly retain the microstructure of the poplar charcoal, but also they exhibited the surprising honeycomb-like mesoporous (2 to 50 nm) alignment in the charcoal templates. This result suggests that the macromolecular chain of the charcoal templates was fractured, sintering at approximately 800 °C in N<sub>2</sub>, further volatilizing the micromolecular materials (CO<sub>2</sub>, CO, and H<sub>2</sub>O) from the charcoal templates (Guo *et al.* 2012). Therefore, it was necessary to repeat the sol-gel process for the C/TiO<sub>2</sub> composites in order to further supply the TiO<sub>2</sub> content and make up the oxygenolysis gaps in the 800C/TiO<sub>2</sub>. The mesoporous structure of the 800C/TiO<sub>2</sub> cell walls may have potential applications for the adsorption for gas or dyes and as a molecular sieve (Kim *et al.* 2009).



**Fig. 5.** SEM of charcoal from mature wood: (a) transverse section (1500× magnification), (b) tangential section (500× magnification), and (c) pitting group (10000× magnification)



**Fig. 6.** SEM of C/TiO<sub>2</sub> composites from poplar sintered at 800 °C: (a) transverse section (100× magnification) and (b) the cell wall with mesoporous (60000 × magnification)

### Dimension Variation

The shrinkage rate (SR) along the radial, tangential, and axial sections were notably anisotropic during the sintering process from the poplar templates to the C/TiO<sub>2</sub> composites (Mizutani *et al.* 2005). Table 1 shows the dimensional variations from the native poplar templates to the 800C/TiO<sub>2</sub> composites. The average SR along the radial, tangential, and axial directions was 28.53%, 21.80%, and 17.03%, respectively. The rule of SR was the SR along the radial direction > the SR along the tangential direction > the SR along the axial direction. In addition, the SR of the average volumes was 53.63%. Therefore, the SR of poplar templates was definitively anisotropic along every direction after sintering to the 800C/TiO<sub>2</sub>.

### CONCLUSIONS

1. Biomorphic C/TiO<sub>2</sub> composites were produced from poplar templates using the sol-gel method and vacuum/positive pressure technology. Consequently, the repetition of infiltrated sol can be decreased through the use of a vacuum/positive pressure technology.
2. Biomorphic C/TiO<sub>2</sub> composites retained exactly the same microstructure of poplar charcoal at 800 °C in N<sub>2</sub>, where the representative pore sizes ranged from 30 to 150 μm, 3 to 15 μm, and 1.5 μm, and exhibited a honeycomb-like mesoporous arrangement.
3. The shrinkage rate of poplar templates was definitively anisotropic along every direction after sintering the poplar templates to the C/TiO<sub>2</sub> composites.

## ACKNOWLEDGEMENTS

This work was financially supported by the National Key Technology R&D Program in the 12th Five-year Plan of China (No. 2014BAK09B03), the Cultured Subject Program of Anhui Agricultural University in China (No. 2014XKPY-36), the Talents Program of Anhui Agricultural University in China (No. wd2015-09), and the Higher Educational Natural Science Foundation of Anhui Province in China.

## REFERENCES CITED

- Chen, X., and Mao, S. S. (2007). "Titanium dioxide nanomaterials: Synthesis, properties, modifications, and applications," *Chemical Reviews* 107(7), 2891-2959. DOI: 10.1021/cr0500535
- Choat, B., Cobb, A. R., and Jansen, S. (2008). "Structure and function of bordered pits: New discoveries and impacts on whole-plant hydraulic function," *New Phytologist* 177(3), 608-626. DOI: 10.1111/j.1469-8137.2007.02317.x
- Colombo, P. (2006). "Conventional and novel processing methods for cellular ceramics," *Philosophical Transactions of the Royal Society A: Mathematical, Physical and Engineering Sciences* 364(1838), 109-124. DOI: 10.1098/rsta.2005.1683
- Deka, B. K., and Maji, T. K. (2011). "Effect of TiO<sub>2</sub> and nanoclay on the properties of wood polymer nanocomposite," *Composites Part A: Applied Science and Manufacturing* 42(12), 2117-2125. DOI: 10.1016/j.compositesa.2011.09.023
- Gu, J., Zhang, G., Dong, S., Zhang, Q., and Kong, J. (2007). "Study on preparation and fire-retardant mechanism analysis of intumescent flame-retardant coatings," *Surface and Coatings Technology* 201(18), 7835-7841. DOI: 10.1016/j.surfcoat.2007.03.020
- Guo, J., Morris, J. R., Ihm, Y., Contescu, C. I., Gallego, N. C., Duscher, G., Pennycook, S. J., and Chisholm, M. F. (2012). "Topological defects: Origin of nanopores and enhanced adsorption performance in nanoporous carbon," *Small* 8, 3283-3288. DOI: 10.1002/sml.201200894
- Kim, J., Tazumi, K., Okaji, R., and Ohshima, M. (2009). "Honeycomb monolith-structured silica with highly ordered, three-dimensionally interconnected macroporous walls," *Chemistry of Materials* 21(15), 3476-3478. DOI: 10.1021/cm901265y
- Kurosaki, F., Ishimaru, K., Hata, T., Bronsveld, P., Kobayashi, E., and Imamura, Y. (2003). "Microstructure of wood charcoal prepared by flash heating," *Carbon* 41(15), 3057-3062. DOI: 10.1016/S0008-6223(03)00434-2
- Li, Y., Fu, Z. Y., and Su, B. L. (2012). "Hierarchically structured porous materials for energy conversion and storage," *Advanced Functional Materials* 22(22), 4634-4667. DOI: 10.1002/adfm.201200591
- Luo, M., Gao, J., Zhang, X., Hou, G., Yang, J., Ouyang, D., Wang, H., and Jin, Z. (2007). "Biomorphic TiN/C ceramics prepared by reduction-nitridation of charcoal/titania composite," *Journal of Materials Science* 42(11), 3761-3766. DOI: 10.1007/s10853-006-0425-9
- Mahr, M. S., Hübert, T., Sabel, M., Schartel, B., Bahr, H., and Militz, H. (2012). "Fire retardancy of sol-gel derived titania wood-inorganic composites," *Journal of Materials Science* 47(19), 6849-6861. DOI: 10.1007/s10853-012-6628-3

- Mizutani, M., Takase, H., Adachi, N., Ota, T., Daimon, K., and Hikichi, Y. (2005). "Porous ceramics prepared by mimicking silicified wood," *Science and Technology of Advanced Materials* 6(1), 76-83. DOI: 10.1016/j.stam.2004.08.004
- Qian, L., Li, R., Zhou, L., Liu, Y., Yu, M., Xiong, F., Liu, S., and Hao, X. (2015). "Preparation of biomorphic TiO<sub>2</sub> ceramics from rattan templates," *BioResources* 10(3), 4391-4402. DOI: 10.15376/biores.10.3.4391-4402
- Shahverdi, M., Dashti, H., and Hossein, M. A. (2012). "Establishing a kiln drying schedule for poplar (*Populus alba* L.) lumber of 7 cm thickness," *BioResources* 7(1), 26-37. DOI: 10.15376/biores.7.1.0026-0037
- Sun, Q., Yu, H., Liu, Y., Li, J., Cui, Y., and Lu, Y. (2010). "Prolonging the combustion duration of wood by TiO<sub>2</sub> coating synthesized using cosolvent-controlled hydrothermal method," *Journal of Materials Science* 45(24), 6661-6667. DOI: 10.1007/s10853-010-4758-z
- Wu, Z., Furuno, T., and Zhang, B. (1998). "Properties of curved laminated veneer lumber made from fast-growing species with radiofrequency heating for use in furniture," *Journal of Wood Science* 44(4), 275-281. DOI: 10.1007/BF00581307
- Yang, D., Liu, H., Zheng, Z., Yuan, Y., Zhao, J. C., Waclawik, E. R., Ke, X., and Zhu, H. (2009). "An efficient photocatalyst structure: TiO<sub>2</sub> (B) nanofibers with a shell of anatase nanocrystals," *Journal of the American Chemical Society* 131(49), 17885-17893. DOI: 10.1021/ja906774k
- Zwieniecki, M. A., and Holbrook, N. M. (2000). "Bordered pit structure and vessel wall surface properties. Implications for embolism repair," *Plant Physiology* 123(3), 1015-1020. DOI: 10.1104/pp.123.3.1015

Article submitted: December 9, 2015; Peer review completed: Peer review completed: February 12, 2016; Revised version received and accepted: February 15, 2016; Published: February 22, 2016.

DOI: 10.15376/biores.11.2.3432-3441